



## A high-rate germanium-particle slurry cast Li-ion anode with high Coulombic efficiency and long cycle life

Kyle C. Klavetter <sup>a,c</sup>, Sean M. Wood <sup>a,c</sup>, Yong-Mao Lin <sup>a,c</sup>, Jonathan L. Snider <sup>a,c</sup>, Nicholas C. Davy <sup>a,c</sup>, Aaron M. Chockla <sup>a,c</sup>, Dwight K. Romanovicz <sup>e</sup>, Brian A. Korgel <sup>a,c,d</sup>, Joo-Woon Lee <sup>a,c,f</sup>, Adam Heller <sup>a,c</sup>, C. Buddie Mullins <sup>a,b,c,d,\*</sup>

<sup>a</sup> Department of Chemical Engineering, University of Texas at Austin, 1 University Station, C0400 Austin, TX 78712-0231, United States

<sup>b</sup> Department of Chemistry and Biochemistry, University of Texas at Austin, 1 University Station, C0400 Austin, TX 78712-0231, United States

<sup>c</sup> Center for Electrochemistry, University of Texas at Austin, 1 University Station, C0400 Austin, TX 78712-0231, United States

<sup>d</sup> Texas Materials Institute, and Center for Nano and Molecular Science, University of Texas at Austin, 1 University Station, C0400 Austin, TX 78712-0231, United States

<sup>e</sup> JCMB Core Lab, University of Texas at Austin, 1 University Station, C0400 Austin, TX 78712-0231, United States

<sup>f</sup> School of Liberal Arts & Sciences, Korea National University of Transportation, Chungju, Chungbuk 380-702, South Korea



### HIGHLIGHTS

- Ge-based slurry cast Li-ion anode performs stably at high C-rates for 2500 cycles.
- Fluoroethylene carbonate (FEC) based electrolyte critical to anode performance.
- Stable performance and near 100% Coulombic efficiency at 10C for 500 cycles.
- $dq/dV$  show thermodynamic reversibility of FEC- but not EC-based electrode.
- Cross-sectional TEM with SEM show structure of cycled anode and SEI.

### ARTICLE INFO

#### Article history:

Received 10 October 2012

Received in revised form

14 January 2013

Accepted 22 February 2013

Available online 14 March 2013

#### Keywords:

Germanium

Li-ion anode

FEC

Fluoroethylene carbonate FEC

Stability toward oxidation

High rate

### ABSTRACT

We report stable, high capacity cycling performance over 2500 deep cycles at variable C-rates (1C, 5C and 10C) for slurry-cast Li-ion battery anodes made using commercially-available germanium nanopowder. The determining factor in cycling performance was the use of fluoroethylene carbonate (FEC) rather than ethylene carbonate (EC) as a co-solvent in the electrolyte. Cycling tests for the FEC-based electrode showed stable performance close to  $700 \text{ mAh g}^{-1}$  through 500 cycles at 10C with near 100% Coulombic efficiency. These results show that a Ge-based slurry-cast electrode using active material structured only as a simple particle can be used to create an electrode system which is a candidate for optimization and scale-up. These cycling improvements obtained using the FEC-based electrolyte complements recent progress in Ge-based electrode research which has focused on improving performance through tailored structural and chemical modifications to the active material structure. The effect of the electrolyte on Li-ion transport, electrode stability toward oxidation, and electrode and SEI structural stability was studied using electrochemical impedance spectroscopy, differential capacity profiles, SEM and cross-sectional TEM imaging where we characterize the evolution of the electrode structure cycled with the FEC-based electrolyte considering the type and extent of SEI growth, particle agglomeration and fracturing.

© 2013 Elsevier B.V. All rights reserved.

### 1. Introduction

High-power and energy-dense lithium-ion batteries are desired for portable electronics and wide-spread adoption to power electric

vehicles. [1] Transitioning from the commercially-used graphite carbon anode ( $372 \text{ mAh g}^{-1}$ ) to metallic silicon, germanium, or various metal oxides could theoretically increase the anode capacity by up to an order of magnitude. However, these electrode materials commonly show capacity fade and inadequate Coulombic efficiencies, particularly at high current densities.

Ge has attracted attention as an alternative anode material because of its large theoretical capacity ( $1384 \text{ mAh g}^{-1}$  or

\* Corresponding author. Department of Chemical Engineering, University of Texas at Austin, 1 University Station, C0400 Austin, TX 78712-0231, United States.

E-mail address: [mullins@che.utexas.edu](mailto:mullins@che.utexas.edu) (C.B. Mullins).

7366 mAh cm<sup>-3</sup> corresponding to Li<sub>15</sub>Ge<sub>4</sub>), [2,3] high electrical conductivity (10<sup>4</sup> times higher than in silicon) [4,5] and exceptional Li<sup>+</sup> ion diffusivity (400 times greater than in silicon at room temperature) [5,6]. Although Ge is about as abundant as tin, there are no concentrated germanium ores and there is very little demand for germanium; for these reasons its price is presently excessive for use in vehicular applications, but applications might be found for mobile electronics requiring long-lasting, energy-dense and high-power batteries.

As in the case of silicon, the repeated volume change in germanium (230%) [5] transitioning to its fully lithiated phase results in large strain gradients that may lead to the cracking and pulverization of particles and the exfoliation of the anode film from the current collector [7,8]. Freshly-exposed fractured surfaces are coated by reduced electrolyte solvents that decompose to form an electrically insulating solid electrolyte interphase (SEI) through irreversible reactions with Li, resulting in both diminished Coulombic efficiency and capacity fade due to slowed Li-ion transport through the surface film and the electrical isolation of fractured material [9–11]. At high current densities, the effects of mechanical strain are more pronounced, leading to poor cycle life as a consequence of particle fracture [5] and a dynamic, continually degrading and reforming SEI resulting from the instability of the Ge-organic electrolyte interface induced by the particle volume changes [12,13].

Nanostructured germanium morphologies for thin films [5,14], nanoparticles [15,16], nanowires [17,18], nanotubes [7], nanocomposites [19,20] and nanocomposite-carbon matrices [21,22] have been investigated in part because small grained materials are known to superplastically deform to accommodate greater than 200% elongation [23–25]. An *in situ* TEM study by Liu et al. showed the mechanical robustness of germanium nanowires (40–125 nm diameter) reversibly cycled between bulk germanium and Li<sub>15</sub>Ge<sub>4</sub> in under 1 min [3]. The nanoscale morphologies better accommodate high strain [26,27], provide shorter Li diffusion distances [28,29] and, as has been demonstrated recently for some Si-based anode designs [30–35], may lead to a more stable SEI/active–material interface.

Advances in the design of germanium anode materials through attention to decreasing Li-ion diffusion distances and improving the structural stability of the particle and SEI have led to exceptional high-rate performance in thin film electrodes [5,14,26,36,37] and more recently to potentially manufacturable slurry cast films [7,16–18,38]. For example, Cho and co-workers reported high rate capacity, slurry cast germanium anodes with stable performance at high rates for up to many hundreds of cycles by using novel nanotube, [7] honeycomb [16] and nanostructured clustered germanium/carbon morphologies [38]. In these electrodes, the Ge particles used were specifically designed for fast Li diffusion and, moreover, were partially or fully shielded from contact with the electrolyte or designed to allow for volumetric expansion away from the SEI into empty space. For the nanostructured clustered germanium/carbon morphologies, after capacity fade from an initial capacity close to 1200 mAh g<sup>-1</sup>, a stable specific capacity of 360 mAh g<sup>-1</sup> was reached after 100 cycles at 40C (64 A g<sup>-1</sup>) [38] and minimal capacity fade was observed for 400 cycles at 0.3/0.6C (0.5/1.0 A g<sup>-1</sup>) lithiation/delithiation rates [7].

Recently, Chockla et al. reported an alternative means to improving the SEI/particle interface stability by using fluorinated ethylene carbonate (FEC) based electrolytes for a slurry cast germanium nanowire-based electrode to achieve stable cycling performance [39]. Here we expand upon this work and similar research into the use of FEC for Si-based electrodes [40–43], studying the evolution of the Ge/EC-based and Ge/FEC-based electrode systems through many cycles with electrochemical testing and detailed study of the electrode architecture by SEM and TEM to demonstrate the effectiveness of the FEC-based electrolyte.

Without the mechanical advantages and short Li-diffusion distances of nanowires as an active material like those used by Chockla et al., and without the improved SEI stability that might otherwise be obtained by using Ge nanostructures intentionally designed to address the repetitive volumetric expansions and contractions that continuously degrade the Ge nanoparticle/SEI interface, [34] we report much improved electrode performance, with higher capacity, Coulombic efficiency and specific power output over longer cycle lifetimes for a slurry cast Ge-based electrode. Made with polydisperse, untailored, commercially-scalable Ge nanopowder and using a FEC-based rather than EC-based electrolyte, the electrode described herein achieves stable performance throughout a 2500 cycle variable, high C-rate test (through nine, successive 200-cycle iterations at 1C, 5C and 10C followed by 700 cycles at 1C, C = 1.624 Ah g<sup>-1</sup>) and a capacity near 700 mAh g<sup>-1</sup> at 10C rate with an average Coulombic efficiency near 100% through 500 cycles. Capacities over 1000 mAh g<sup>-1</sup> were observed when discharging the electrode at up to 20C while charging at 1C and a capacity of 425 mAh g<sup>-1</sup> was achieved for a discharge rate of 50C. These results complement the recent progress in slurry cast Ge-based electrode research which has focused on improving cycling performance through structural and chemical modifications to the active material. The notable cycling stability of the electrode in FEC-electrolyte, sustained through both extended cycling and high C-rate testing, indicates that the improved performance may be found in the role of FEC forming a SEI that better protects the Ge nanoparticle active material from contact with the electrolyte, a consequence of the different surface films likely rich in lithium fluoride, alkoxy and polycarbonate species which have been found to be the result of FEC reduction [42,44]. This results in higher CE as a consequence of a more stable SEI/particle interface, and, from considering the evolution of the electrode differential capacity profiles, an enhanced stability toward oxidation that significantly delays capacity fade and corresponding oxidation of the Ge nanoparticle active material, a finding analogous to the result recently reported by Etacheri et al. in their study on FEC and Si NW [44]. Herein we report how the FEC-based electrolyte with a Ge-based electrode is an effective means to improving the SEI so as to minimize irreversible losses and better protect the Ge nanoparticle from oxidation, thereby improving the battery performance parameters of interest: long cycle life, specific capacity, capacity retention, Coulombic efficiency and high C-rate capability.

## 2. Experimental

### 2.1. Ge nanoparticle electrode preparation and battery assembly

Ge nanoparticles (99.9%, American Elements) were used as the active material in the electrode. The reported average particle size was 70–120 nm. However, the actual particle size distribution ranged up to several microns (a typical TEM of Ge particles after dispersing via bath sonication is shown in [Supplementary Information Figure SI.1](#)). Slurries of 40:20:40 w/w/w Ge nanoparticles:poly-acrylic acid binder (PAA-450 kDa, Sigma):Super-P Li conductive additive (Timcal) with ethanol as solvent were cast on a copper foil current collector to prepare the electrode for battery testing. This film composition, made of a high weight fraction of conductive additive, was selected to diminish the effect on cycling performance of losing a sustained electrical percolating network as a consequence of particle shifting due to the volumetric expansion and contraction of the Ge nanoparticles during cycling after preliminary screening for slurry compositions with a film composed of 80:10:10 w/w/w (Ge nanoparticles:PAA-450 kDa:Super-P Li conductive additive) showed capacity fade after only 100 cycles at a rate of 1C: 0.49 mAh g<sup>-1</sup> (or 0.05%) capacity fade per cycle with an areal capacity

of  $0.26 \text{ mAh cm}^{-2}$  (Supplementary information Figure SI.2). The contribution of this high content of conductive additive to the specific capacity of the 40:20:40 w/w/w electrode was estimated to be near ten percent (Supplementary information Figure SI.3). For the electrode binder, PAA, demonstrated to have enabled better cycling stability for Si-based electrodes [45], was selected rather than the typically polyvinylidene fluoride (PVDF) after a preliminary binder screening cycling test (Supplementary information Figure SI.4). In a typical procedure, the slurry is mixed and probe-sonicated (1/4" tip, QSonica) prior to being doctor-bladed onto Cu foil. The film is dried overnight at  $120^\circ\text{C}$  and then 11 mm diameter circular electrodes are hole-punched. The typical electrode mass loading used here of  $300\text{--}500 \mu\text{g cm}^{-2}$  delivers an areal capacity of  $0.15\text{--}0.06 \text{ mAh cm}^{-2}$  (for 1C–10C rates), an order of magnitude lower than current commercial anodes such as the 18650 cell ( $4 \text{ mAh cm}^{-2}$ ) [46]. From TEM cross-sectional imaging (Supplementary information Figure SI.5) the electrode density is estimated to be near  $0.9 \text{ mg cm}^{-3}$  ( $0.35 \text{ mg of Ge nanoparticle/cm}^3$ ). The electrodes are assembled in an Ar-filled glovebox ( $<0.1 \text{ ppm O}_2$ ) with a Li foil (Alfa) counter/reference electrode and Celgard 2400 membrane separator ( $25 \mu\text{m}$  in thickness) in 2032 stainless steel coin cells. The effect of the Li-plating/dissolution kinetics in the electrolytes studied herein, particularly at high current densities, was evaluated (Supplementary information Figure SI.6) by testing coin cells made of two electrodes of Li foil assembled in a similar manner as for the Ge nanoparticle based electrodes. The electrolyte was composed of either 1 M LiPF<sub>6</sub> ( $\geq 99.99\%$ , Aldrich) in ethylene carbonate/di-methyl carbonate (EC/DMC, 1:1) (LP30, EMD Chemicals), selected as representative of the conventionally used EC-based electrolytes for the typical Ge-based electrode, or 1 M LiPF<sub>6</sub> in FEC ( $>99\%$ , Solvay Fluor)/diethyl-carbonate (DEC,  $\geq 99\%$ , Aldrich) (1:1, v/v), the electrolyte shown by Chockla et al. to have enabled the best cycling performance [39]. The Solvay product was used because FEC procured from MTI and TCI America was observed to decompose into a black-colored liquid. To assess the performance of electrodes made using more active material and with higher mass loadings (greater than  $1300 \mu\text{g cm}^{-2}$ ), additional cycling tests (Supplementary information Figure SI.7) were done with a slurry of 60:20:20 w/w/w Ge nanoparticle:PAA:Super-P Li conductive additive.

## 2.2. Electrode characterization

Scanning electron microscopy (SEM) images were acquired using a Hitachi S5500 SEM with an accelerating voltage of  $10 \text{ kV}$  and current of  $20 \mu\text{A}$ . The electrodes were prepared for SEM after soaking in DMC overnight and were exposed to air for less than 60 s during transfer from a vacuum transfer box into the SEM high vacuum chamber. Transmission electron microscopy (TEM) images were acquired using either a FEI Tecnai Spirit BioTwin TEM operated at  $80 \text{ kV}$  or a field emission JEOL 2010F TEM operated at  $200 \text{ kV}$ . TEM samples were prepared by ultramicrotome sectioning of epoxy-embedded electrodes to  $50\text{--}70 \text{ nm}$  thicknesses using a diamond knife (35° Ultra, DiATOME). A detailed description of the sectioning procedure is provided in the Supporting information.

An electrochemical analyzer (CHI 604D, CHInstruments) was used for electrochemical impedance spectroscopy (EIS), measured over a wide frequency range from  $100 \text{ kHz}$  to  $0.001 \text{ Hz}$  with an AC perturbation voltage of  $5 \text{ mV}$ . Cells were poised at the selected potential for longer than 5 min before taking the spectra.

The electrode performance was measured using a multichannel battery test system (BT 2043, Arbin) to run cycling tests with constant current between  $0.01$  and  $1 \text{ V}$  vs  $\text{Li}/\text{Li}^+$ . For all tests done, a conditioning cycle at  $C/20$  was run in order to form a consistent SEI prior to commencing the testing schedules at high C-rates. Capacity values are reported as the Li-extraction capacity and are based

upon active material only. Although  $\text{Li}_{15}\text{Ge}_4$  is the ultimate phase thermodynamically achievable for electrochemistry done at room temperature, for the convenience of the reader who might compare these results with those in previous literature, the cycling rates are reported based on the  $\text{Li}_{22}\text{Ge}_5$  theoretical capacity, i.e.,  $1\text{C} = 1624 \text{ mAh g}^{-1}$ . The specific capacity values reported in the text are gravimetric, specific to the mass loading of the Ge nanoparticles in the electrode. For the cycling data presented in graphical form, the specific gravimetric capacity, specific to the mass loading of the Ge nanoparticles and also, as denoted in bracketed values on the primary ordinate axis, specific to the mass loading of the electrode film (made of Ge nanoparticles, binder and conductive additive), is provided. The CE values are reported with an uncertainty of up to 0.2%, reflecting the level of accuracy in current measurement on the Arbin battery testers. Four separate Arbin battery tester units were used to test cells in an effort to increase confidence in the repeatability of the reported data and also in order to minimize the extent to which instrument error impacted the reported data; the CE values reported for the selected tests are representative of several results from each Arbin tester used. The terms charge and discharge are used as they would be for a full Li-ion cell, with discharge referring to Li-extraction from the Ge electrode.

## 3. Results

### 3.1. Ge Nanoparticle Li-Ion Cell performance

Li-ion cells with Ge nanoparticle anodes were tested using polyacrylic acid (PAA) binder, conductive carbon (2:1:2 w/w/w Ge:PAA:C) and 1.0 M LiPF<sub>6</sub> electrolyte in two mixtures of carbonates. Fig. 1 shows the reversible capacity of electrodes cycled 600 times between  $0.01$  and  $1 \text{ V}$  vs  $\text{Li}/\text{Li}^+$  at a rate of 1C (200 cycles), 5C (200 cycles) and 10C (200 cycles). As reported [18,41,47], the use of fluorinated carbonates as co-solvents or as additives was found to improve electrode performance, resulting in stable performance, higher Coulombic efficiencies and higher capacities. During the first cycle, the electrode tested in FEC:DEC showed marginally improved CE compared to when tested in EC:DMC, 50.5% vs. 45.1%, likely reflecting a thinner SEI as has been reported by others for Si-based systems tested with FEC [43,44]. After 200 cycles at 1C, the anode cycled in FEC:DEC yielded a capacity of  $1152 \text{ mAh g}^{-1}$ , corresponding to a negligible gain of 0.18% relative to the 10th cycle. (The 10th cycle was selected as the basis for comparison because the cycling behavior for the electrode showed capacity increase during the first several cycles before reaching a relatively stable value: selecting an earlier cycle than the 10th would artificially inflate the

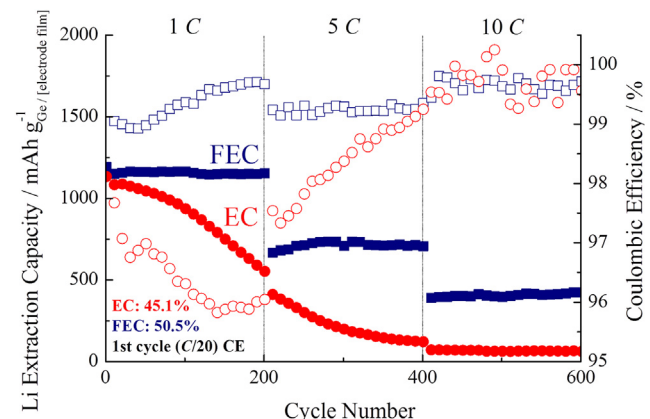


Fig. 1. Cycling performance of Ge nanoparticle electrodes tested at 1C, 5C and 10C in EC/DMC and FEC/DEC electrolytes.

capacity retention values reported.) During this period, the Coulombic efficiency increased from 99.1% to 99.7%. From the 10th to 200th cycle, the anode tested in EC/DMC showed significant capacity fade, decreasing from 1083 to 552  $\text{mAh g}^{-1}$ , and its Coulombic efficiency fell from 97.7% to 96.0%. Through the first 200 cycles of testing, the electrode cycled in EC/DMC is calculated to have accumulated greater than 2  $\mu\text{g}$  of Li per  $\mu\text{g}$  of Ge nanoparticle as a result of irreversible losses. By comparison, through the same number of cycles, the electrode cycled in FEC/DEC accumulated only 0.74  $\mu\text{g}$  of Li per  $\mu\text{g}$  of Ge nanoparticle, with 41% of this irreversible consumption of Li occurring during the first cycle (as compared with only 17.5% for the electrode cycled in EC/DMC). Even after 2500 cycles of testing at variable C-rates, the electrode cycled in FEC/DEC only accumulated marginally higher irreversible losses than the electrode cycled in EC/DMC for 200 cycles: 2.4 vs 2.0  $\mu\text{g}$  of Li per  $\mu\text{g}$  of Ge nanoparticle.

At higher rates, the differences in performance were more pronounced. From the 210th to 400th cycles run at 5C, the anode cycled in FEC/DEC retained over 60% of the 1C capacity and cycled stably, showing a slight increase in capacity from 667 to 706  $\text{mAh g}^{-1}$ . During this period, the anode cycled in EC/DMC showed continued capacity fade from 410 to 121  $\text{mAh g}^{-1}$ . From the 410th to 600th cycles run at 10C, the anode cycled in FEC/DEC retained about 35% of the 1C capacity and cycled stably, showing a slight increase in capacity from 389 to 423  $\text{mAh g}^{-1}$ . When at 10C, the anode cycled in EC/DMC showed very low capacities, ranging from 72 to 62  $\text{mAh g}^{-1}$ .

Long-cycle life was also observed for the electrode cycled 500 times in the FEC/DEC electrolyte at 10C. Interestingly, a separate cycling test (Fig. 2a) showed that the anode cycled in FEC/DEC demonstrates capacities of near 700  $\text{mAh g}^{-1}$  and high Coulombic

efficiencies between 99.8 and 100.2% when tested for 500 cycles at 10C without prior extended cycling. These results were also found for a variable rate test done at 1C, 5C and 10C when the anode cycled only 100 times at each rate (Supporting information Figure SI.8). From the 10th to the 100th cycle tested at 1C, there was an increase in capacity from 1144 to 1186  $\text{mAh g}^{-1}$  with a corresponding increase in Coulombic efficiency from 99.2% to 99.3%. During the 110th to 200th cycles run at 5C, the anode retained 75% of the 1C capacity and cycled stably, showing an increase in capacity from 870 to 929  $\text{mAh g}^{-1}$  and Coulombic efficiencies between 99.7 and 99.9%. When tested at 10C in FEC/DEC, the electrode retained over 53% of the 1C capacity and cycled stably, showing an increase in capacity from 631 to 657  $\text{mAh g}^{-1}$  and lower Coulombic efficiencies between 99.0 and 99.4%. Electrodes tested at these and other high rates in the EC/DMC electrolyte were observed to perform poorly, showing either negligible capacities or severe capacity fade.

These cycling results done with commercial Ge nanoparticles in an electrode matched with an FEC-based electrolyte build upon the recent body of work done in improving the state of Ge-based slurry-cast anodes, notably by Park et al., who reported only minimal capacity fade for a Ge nanotube based anode from an initial value near 1000  $\text{mAh g}^{-1}$  through 400 cycles at 500  $\text{mA g}^{-1}$ /1000  $\text{mA g}^{-1}$  ( $\sim 0.3/0.6\text{C}$ ) charge/discharge high rate, although capacity fade from near 750  $\text{mAh g}^{-1}$  was observed over the 5 cycles shown at 1000  $\text{mA g}^{-1}$  ( $\sim 0.6\text{C}$ ). [7] Chockla et al. recently reported [18] capacities of  $>1000 \text{ mAh g}^{-1}$  after 300 cycles for a Ge nanowire based anode using a current density of 138  $\text{mA g}^{-1}$  ( $\sim \text{C}/12$ ). When tested at 1.38  $\text{A g}^{-1}$  ( $\sim 0.85\text{C}$ ) the capacity dropped but was stable near 700  $\text{mAh g}^{-1}$  for over 1000 cycles. Seng et al. reported impressive high rate capabilities up to 40C but still capacity

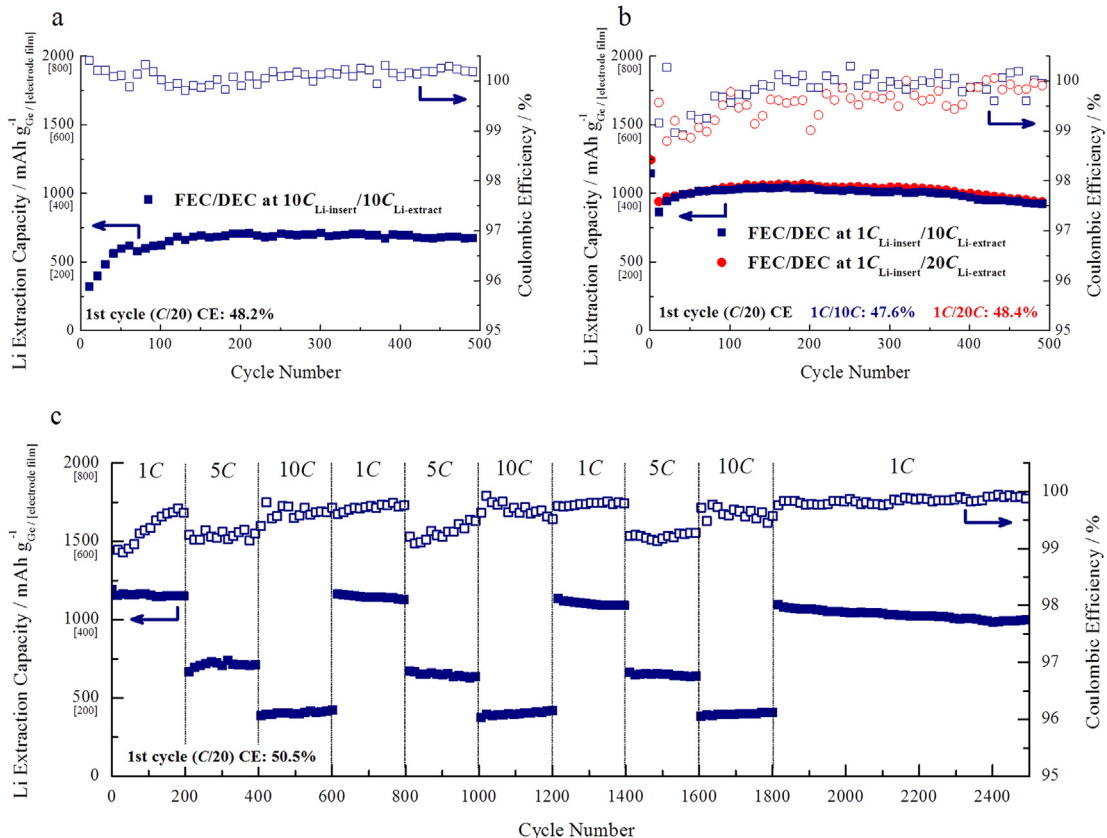


**Fig. 2.** Cycling performance of Ge nanoparticle electrode cycled in the FEC/DEC electrolyte (a) at 10C, (b) at 10C or 20C discharge rate with 1C charge rate and (c) at intervals of 1C, 5C and 10C through 2500 cycles.

fade was evident at all rates, with the capacity retention at 1C testing being 74% after 120 cycles [38]. Xue et al. reported observing 50 cycles at high capacities but with capacity fade and low Coulombic efficiencies (91%) for a nanocomposite anode cycled at 1600 mAh g<sup>-1</sup> (1C) [20].

### 3.2. High C-rate performance

For certain applications requiring high current densities such as in the acceleration of an electric vehicle, the capability to rapidly discharge the anode is desired. The Ge nanoparticle based electrodes in FEC/DEC were subjected to long-term cycling tests with two discharge rates in which the charge rate was held constant at 1C. This test was done because the Li transport through the SEI and Li-insertion process is known to be the limiting step in the cycling of the cell, where Li plates on the surface of the particles when charged above a critical current density, as is similarly the case for the graphite-based anode [48]. When the highly charged Ge nanoparticles were discharged, unlike for the graphite anode which undergoes small volumetric contraction during de-intercalation of its stored Li, the Ge nanoparticles' volumetric contraction during these high C-rate tests is estimated to be near the theoretical value given the high capacities observed (near 1000 mAh g<sup>-1</sup>). Despite the strain endured during the short time allowed for the morphological transition for these tests, the Ge nanoparticles perform with high capacity and high CE through many cycles, suggesting that the FEC-derived SEI enables a stable SEI/particle interface. As was shown by Chockla et al. [39] for Ge nanowire-based slurry cast films, we observed good capacity retention for a discharge rate of 10C or 20C (Fig. 2b) through 500 cycles, and also with very high capacity retention for the electrodes discharged at different rates. The maximum capacity attained for the 10C discharge rate anode was 1049 mAh g<sup>-1</sup> (cycle 170) and the 20C discharge rate anode was 1069 mAh g<sup>-1</sup> (cycle 191) after which gradual capacity fade was observed. The capacity retention at the 500th cycle for the 10C discharge rate anode was 86.8% of the maximum value and the 20C discharge rate anode was 87.7%. For both cells, the fast rate of Li-extraction led to high Coulombic efficiencies, averaging 99.8% (10C) and 99.6% (20C) from the 5th to 500th cycles. When the cell was discharged at 50C rate (discharge completed in 19 s), we observed a capacity near 425 mAh g<sup>-1</sup> for close to ten cycles (Supplementary information Figure SI.9). After this initially stable cycling performance, this rapid discharge testing (at 50C) resulted in unusual behavior in which the Li-extraction capacity gradually increased and exceeded the Li-insertion capacity for each cycle through the 250th cycle. It is conceivable that overheating damaged the separator membrane [49] or that the high overpotential required for Li plating during discharge was the cause of this result. Further testing done using Li foil treated with tetraethyl orthosilicate [50], a process intended to minimize the growth of dendrites and to diminish impedance of Li<sup>+</sup> ion transport at the Li foil, showed improved cycling stability at this high discharge rate (Supplementary information Figure SI.10).

### 3.3. Long-term cycling performance and stability

Long term stability was examined for the Ge-nanoparticle-based electrode cycled in FEC/DEC using a 2500 cycle test with sequential 200 cycle intervals at rates of 1C, 5C and 10C (Fig. 2c). A table detailing the performance and capacity retention of this electrode may be found in the Supplementary information Table SI.1. Because the useful lifetime of a battery is measured by the cycles for which its capacity retention is greater than 80% [51], the capacity retention after the second, third and fourth sets of 1C testing is considered here and found to be 97.8%, 94.8% and 87.0%

(through 800, 1400 and 2500 cycles, respectively) as compared to the capacity achieved during the initial 1C testing after the electrode attained a relatively steady capacity by cycle 10. For this extended cycling, the Coulombic efficiency was marginally improved from nearly 99.7% to fractionally above 99.8% for cycles 800, 1400 and 2500. We observed that during the third set of 1C cycling (from cycles 1200–1400), the electrode performance improved after showing a typical rate of capacity fade (about 0.4 mAh g<sup>-1</sup> per cycle), stabilizing between cycles 1330 and 1400. Through these cycles there was less than 2 mAh g<sup>-1</sup> total capacity fade (corresponding to a 0.1% change, shown in red-lined box, a, in Fig. 2c and in Supplementary information Figure SI.11a). This stable cycling performance continued through over the next 100 cycles tested at 5C (shown in the orange-lined box, b, and in Supplementary information Figure SI.11b) before gradual capacity fade at a rate of about 0.25 mAh g<sup>-1</sup> per cycle resumed. When testing at 10C (shown in the green-lined boxes, c), we observed that the cycling performance showed marked capacity increase throughout each 200 cycle series. It may be that this better-than-stable-cycling behavior is due to minimal fracturing of the SEI/Ge nanoparticle interface which undergoes limited volumetric expansion when the Ge nanoparticles are being only partially lithiated at this high C-rate.

### 3.4. Voltage profiles, differential capacity plots

Fig. 3 shows the voltage profiles at variable high C-rates for Ge-nanoparticle electrodes cycled in the EC/DMC and FEC/DEC electrolytes. Information about the evolution of bulk Li<sub>x</sub>Ge phase transitions and the irreversible reactions, particularly the formation of the SEI, is obtained from the voltage profiles shown in differential form (Fig. 4). The contribution of the Li foil to the overpotential required to charge/discharge the electrode is estimated to be near half of the operating voltage measured for the stripping/plating of Li in coin cells made using the EC and FEC based electrolytes with Li foil as both the positive and negative electrodes (Supplementary Figure SI.6). When at high current densities (approximating the 10C rate tests done on the electrodes of relatively small mass loadings reported here), the overpotential required for plating/stripping of Li begins to become significant and is estimated to be near 75 mV. Notably, cycling the Li vs Li cells tested in FEC:DEC consistently required higher overpotentials than those tested in EC:DMC.

The first cycle differential capacity profile (Fig. 4) shows that both electrodes possess the same sequence of Li-insertion and Li-extraction features. The initial reduction of the electrolyte to form SEI is shown in Supplementary information Figure SI.12a. As has been reported previously for a Si-based anode [43], the reduction of FEC begins at a lower overpotential than that for EC. After this initial SEI formation feature occurs, another larger irreversible feature near 550 mV (highlighted in the green-lined box, marked a) which for the electrode cycled in EC/DMC is broader and larger than that for the electrode cycled in FEC/DEC. This corresponds to the lower first cycle Coulombic efficiency reported for the EC/DMC electrode, 45.1% vs 50.5% (at C/20) for the electrode cycled in FEC/DEC.

For the first cycle, the Li insertion behavior is changed depending upon the electrolyte used, as depicted in Fig. 4. The first Li insertion feature at 310 mV (highlighted in the blue-lined box, b) for the electrode cycled in EC/DMC is smaller in magnitude, both in comparison to the feature of the electrode cycled in FEC/DEC and when compared to the second Li insertion feature at 175 mV. These two Li-insertion peaks likely correspond to the two-step mechanism through which Li first inserts as a nearest neighbor to Ge in the Ge crystal lattice prior to a second wave of Li insertion to sites where Li is primarily surrounded by other Li [52]. As reported by Baggetto et al. [9] in their in-situ XRD study of deposited Ge thin

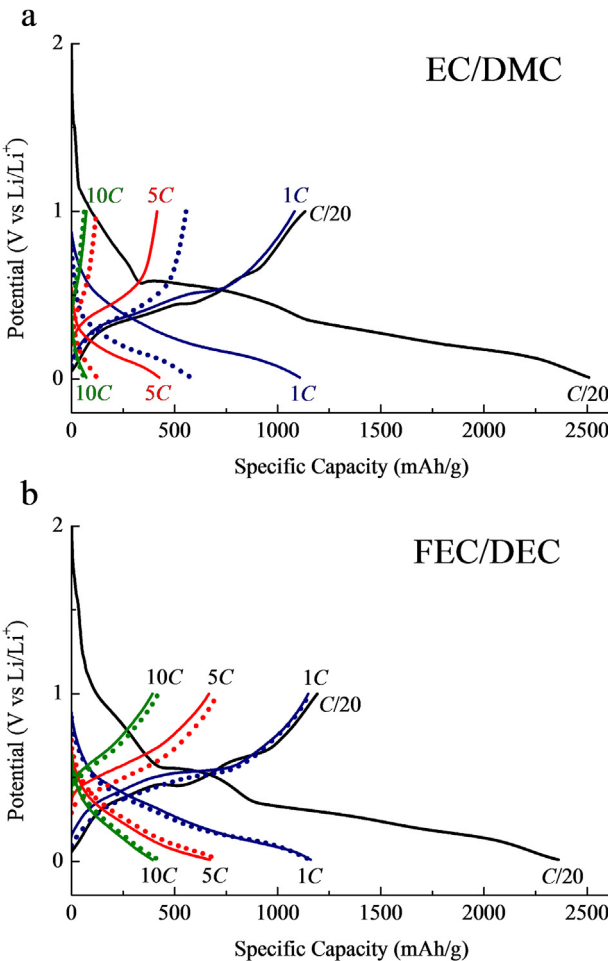


**Fig. 3.** Voltage profile for Ge nanoparticle electrode cycled in EC/DMC for 601 cycles: 1 conditioning cycle at C/20 followed by 200 cycles at 1C, 200 cycles at 5C and 200 cycles at 10C with (a) EC/DMC as the electrolyte and (b) FEC/DEC as the electrolyte. Solid/dotted lines represent data from the 10th/200th cycle in each series.

films, no known  $\text{Li}_x\text{Ge}$  crystalline phase forms (although several amorphous transitions were believed to have been observed) during the Li-insertion process before the ultimate thermodynamically-accessible phase,  $\text{Li}_{15}\text{Ge}_4$  is attained between 130 and 30 mV, a finding with which the small Li-insertion feature observed in this study near 50 mV is consistent. Additionally, Baggetto et al. reported evidence for short range ordering of the  $\text{LiGe}$  and then  $\text{Li}_7\text{Ge}_2$  phases [2] through making measurements of Ge–Ge and Ge–Li interatomic distances using in-situ X-ray absorption spectroscopy during Li-insertion. These phases may correspond to the two defined Li-insertion peaks observed in this study near 120 and 75 mV. The two prominent Li-extraction features may be explained by the reversal of these phase transitions, proceeding back to de-lithiated Ge nanoparticles via the  $\text{Li}_{15}\text{Ge}_4/\text{Li}_7\text{Ge}_2$  phase transition (near 360 mV) and  $\text{Li}_7\text{Ge}_2/\text{LiGe}$  phase transition (near 530 mV).

In the first cycle, the Li extraction behavior for the electrodes tested in the two different electrolytes is similar in kind, but not in magnitude, with a larger fraction of the Li extraction occurring for the electrode cycled in EC/DMC at the feature near 350 mV (highlighted in the black-lined box, c). This extraction feature corresponds to the larger insertion feature seen in the EC/DMC electrode at 175 mV. At 450 mV, a sharp peak appears superimposed on the broader Li extraction feature with its peak at 350 mV. This sharp feature, also observed by Chockla et al., [18] has little magnitude and is observed for both electrode systems, possibly corresponding

to a two-phase transition in which Li extracts from the small amount of crystalline  $\text{Li}_{15}\text{Ge}_4$ . Although the major Li-insertion features are observed with 135 mV spacing, the last significant oxidation feature is observed near 630 mV, close to 280 mV after the first extraction feature, and in subsequent cycles this feature does not appear. For the electrode cycled in FEC/DEC, a small shoulder feature is observed at 750 mV, and, for the electrode cycled in EC/DMC another feature is observed to grow as the upper voltage limit (1.0 V vs.  $\text{Li}/\text{Li}^+$ ) is approached (Supplementary information Figure SI.12b). The location of these two minor features appearing at high potentials and exclusive to the first cycle suggests that they may represent the partial oxidation of the large amount of SEI formed in this cycle.

The second cycle differential capacity profiles reflect the lithiation of a more amorphous material, showing broad Li-insertion features with peaks at 120 mV and 75 mV for the electrodes cycled in EC/DMC and FEC/DEC respectively. For both electrodes, although more noticeably for the electrode cycled in FEC/DEC, a shallow, broad feature was observed between 500 and 250 mV. The Li-extraction for the electrode cycled in EC/DMC began at 140 mV, far lower than the 227 mV for the electrode cycled in FEC/DEC. This difference in the initial discharge potential was seen throughout the 200 cycles examined and reflects significant differences in the polarization of the two electrode/electrolyte systems after Li-insertion. The higher potential at which the differential capacity profile begins for the electrode tested in FEC/DEC may reflect a more rapid Li-diffusion rate of Li deposited or alloyed near the surface of the active material particles into the bulk of the material. By the 200th cycle this disparity in the polarity between the two electrodes following Li insertion was lessened to about 15 mV as a result of the initial discharge potential for the electrode tested in FEC/DEC decreasing throughout testing. After the electrode cycled in EC/DMC began to exhibit significant capacity fade after about its 50th cycle, a similar divergence between the electrodes in their initial charging potential was observed. From the 50th to 200th cycles, the initial charging potential for the electrode tested in EC/DMC following Li extraction decreased from 857 mV to 770 mV while that of the electrode cycled in FEC/DEC only marginally decreased from 883 to 859 mV, indicating more facile Li extraction for this electrode system. The plot of the relaxation currents for the cycles discussed here may be found in Supplementary information Figure SI.13.

Throughout the first 20 cycles, during which there was a marginal increase in capacity for both electrodes, the Li-insertion features for the electrode cycled in FEC/DEC continuously evolved as its primary Li-insertion peak shifts to lower overpotentials, from 75 mV (cycle 2) to 140 mV (cycle 20). The shift of this peak in the electrode cycled in EC/DMC was less pronounced, from 120 mV (cycle 2) to 160 mV (cycle 20). Although there were as many as three identifiable Li-insertion features observed for the FEC/DEC electrode (cycle 5), by cycle 20, these merged into one broad, flat feature that remained constant throughout the remainder of the 200 cycle testing. This observation suggests that after the first several cycles, the successive phase transitions from the initially crystalline Ge proceeded through amorphous  $\text{Li}_x\text{Ge}$  phases, not through alloys with long-range lattice order that would transition through distinct voltage windows. During these first 20 cycles, the Li-extraction features for both electrodes were relatively constant. At cycle 20, a smaller, broader feature was seen at 360 mV for the EC/DMC electrode before a sharper peak at 515 mV. For the electrode cycled in FEC/DEC, a broad shoulder rather than distinguishable peak was observed, beginning at 285 mV before merging with the sharp peak (530 mV) similar to that seen in the profile for the EC/DMC electrode.

After the 20th cycle, as capacity fade in the electrode cycled in EC/DMC became evident, the Li-extraction behavior for this system notably changed. Highlighted by the red-lined boxes (labeled d–g)

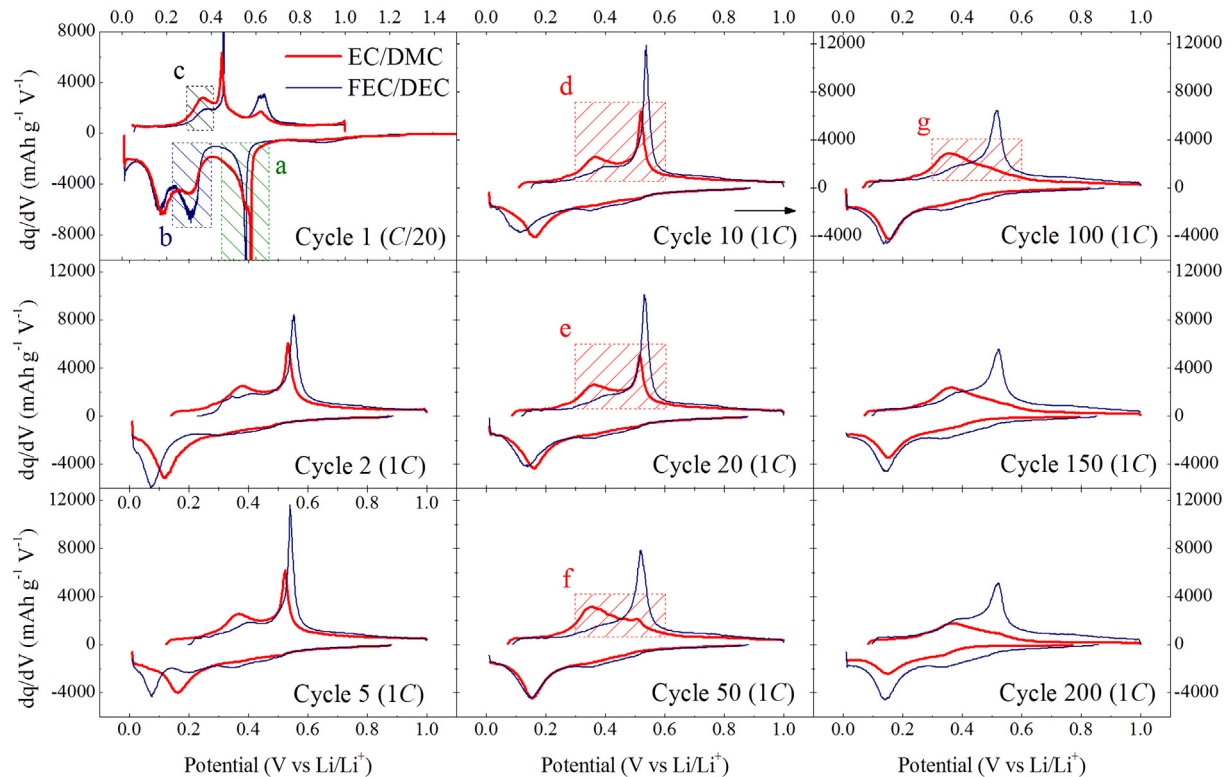


**Fig. 4.** Differential capacity profiles for Ge nanoparticle electrodes cycled in EC/DMC (red line) and FEC/DEC (blue line) with the initial cycle at C/20 and the remaining 199 cycles at 1C. (For interpretation of the references to color in this figure legend, the reader is referred to the web version of this article.)

in Fig. 4, the ratio of the magnitude of the broad feature (360 mV) to the sharp peak (515 mV) increased, with most of the Li extraction occurring at lower potentials. By cycle 100, there was no noticeable peak near 515 mV, although the Li insertion behavior for the electrode remained unaltered. After cycle 100, there was only a change in magnitude, not a change in kind, of the differential capacity profile for the electrode cycled in EC/DMC. The features present in the 100th cycle profile diminished in magnitude in proportion to one another. In contrast to the change in the Li-extraction behavior for the EC/DMC electrode, the differential capacity profiles reflect the enhanced cycling stability of the FEC/DEC electrode. By the 200th cycle, the sharp peak observed in cycle 20 had broadened but otherwise the features remained nearly identical in both magnitude and shape. The significance of this difference in the differential capacity profiles between the two electrode systems is further discussed in Section 4.2.

In Fig. 5, differential capacity profiles are shown for the last cycle in each of the 200 cycle series that made up the long-term cycling test for the FEC/DEC electrode. The three nearly identical 1C profiles (separated by intervals of 600 cycles of cycling at 5C, 10C and then 1C) shown for the electrode demonstrate the thermodynamic reversibility of this electrode system. There was a slight attenuation in the amplitude of the profile of the 800th cycle compared with that observed for the 200th cycle, reflecting the lower capacity (97.8% capacity retention comparing cycles 800 to 200). Likewise, the profile of the 1400th cycle almost exactly overlaid that of the 200th cycle, with a capacity retention close to 94.8% (compared to cycle 200). A similar result was observed in comparing the 400th, 1000th and 1600th cycles (tested at 5C) and the 600th, 1200th and 1800th cycles (tested at 10C), where the profiles of the differential capacity plots remained were observed to change only in magnitude, with a small decrease in the amplitude of their features.

During the last seven-hundred cycles ending at cycle 2,500, sustained capacity fade on the order of 0.1 mAh g<sup>-1</sup> per cycle is observed, and the differential capacity profile shows that the sharp Li-extraction feature near 500 mV has largely disappeared in a manner similar to the behavior of this same feature for the electrode cycled in EC/DMC electrolyte through 200 cycles. For both

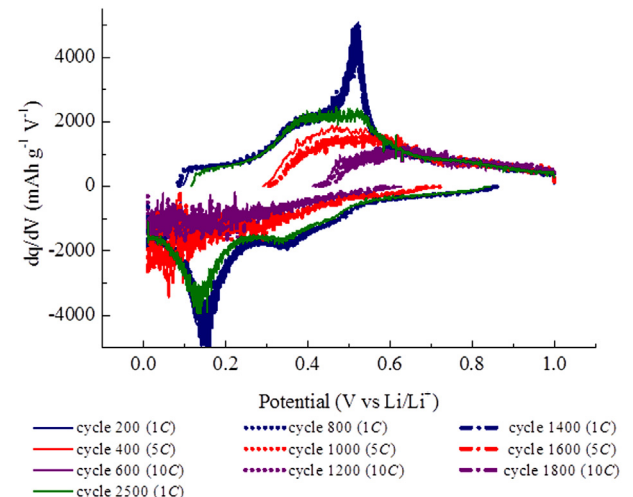


**Fig. 5.** Differential capacity profiles for Ge nanoparticle electrodes cycled in FEC/DEC after 1C (blue lines), 5C (red lines), 10C (purple lines) after the first (solid line), second (dotted line) and third (dashed line) cycle sets. The green line indicates the differential capacity profile for the 2,500th cycle, after 700 cycles at 1C following the third set of high rate testing. (For interpretation of the references to color in this figure legend, the reader is referred to the web version of this article.)

electrodes, the preservation of this feature correlates with stable cycling performance, and we here suggest that the decay of this feature and the corresponding capacity fade in the electrode may be related to the rate of oxidation of the germanium active material. As has been shown by Etacheri et al. [40] in their excellent study on the effect of FEC on Si-nanowire anodes, reported by Choi et al. [43] when considering FEC as an electrolyte additive and observed by Nakai et al. [42] in their detailed XPS depth profiling of evaporated thin Si-films, the fluorinated electrolyte solvent may stabilize cycling performance by minimizing the extent to which the active material oxidizes during cycling, a reaction likely resulting from the presence of trace concentrations of water in the coin cell and electrolyte. A comparison of the electrode cycled in FEC:DEC after 2500 cycles and of the electrode cycled in EC:DMC after 200 cycles to a similarly prepared  $\text{GeO}_2$ -based slurry cast electrode (Supplementary information Figure SI.14b) indicates that after cycling has progressed to the onset of significant capacity fade, the Ge nanoparticle may have become partially oxidized—albeit at a far slower rate for the electrode cycled in FEC:DEC than in EC:DMC—and to the extent that the partially oxidized Ge nanoparticle-based electrode's thermodynamic Li-insertion and Li-extraction pathways closely resemble those of the  $\text{GeO}_2$  nanoparticle-based electrode, the Li-insertion and Li-extraction features matching in both location (potential) and amplitude (Supplementary information Figure 15).

### 3.5. Electrochemical impedance spectroscopy

The information provided by differential capacity profiles can be supplemented by the results of electrochemical impedance spectroscopy (EIS) taken at intervals throughout galvanostatic testing in order to provide a more comprehensive picture of the evolution of the nominally identical Ge nanoparticle-based anodes cycled using different electrolytes. Differential capacity profiles provide a means to locate and determine the extent of the chemistry of surface film growth and the lithiation of the Ge nanoparticle. The surface film formed by the reduction of electrolyte can be a significant variable in explaining the observed differences in cycling performance between the nominally identical anodes tested in the two different electrolytes. EIS can be used to analyze properties related to the chemistry, morphology and thickness of this surface film, which are factors which limit the extent of lithiation of the Ge nanoparticle due to added impedance regarding  $\text{Li}^+$  ion transport and charge transfer.

The impedance of the transport of Li-ions through multilayered surface films is modeled as a series of parallel resistor/capacitor ( $R||C$ ) circuits represented in the spectra as semicircles in the high and medium frequency regions and a Warburg resistance represented as a sloped line in the low frequency region. The very high frequency region that describes the impedance through the electrolyte and separator membrane is observed as a combined resistor, measured as the resistance up to the beginning of the first semicircular feature. The diameter of the high frequency semicircle corresponds to impedance regarding  $\text{Li}^+$  ion migration through the SEI, and the diameter of the medium frequency semicircle corresponds to charge transfer resistance at the interface of the SEI and active material surface.

Due to the complexity of the slurry-cast anode, these impedances must be represented by constant phase elements in the equivalent circuit, reflecting the non-ideality of the system arising from (a) the surface roughness and 3D morphology of the electrode, (b) the distribution of reaction rates on the Ge nanoparticle surface (a consequence of uneven SEI growth, asymmetric particle geometry and the random orientation of the active and inactive materials in the film), (c) the varying thickness of the film and non-uniform

composition due to imperfect mixing of the slurry and (d) non-uniform current distribution (both in the subject electrode and on the  $\text{Li}/\text{Li}^+$  foil counter/reference electrode surface due to dendritic growths). The initial linear profile of the spectra in the low frequency region is attributed to impedance resulting from solid state Li diffusion limitations. The steeper sloped linear profile in the very low frequency region is due to insertion capacitance. The low frequency region of the spectra is generally not considered when comparing electrolyte effects because it is assumed that the bulk properties of the cycled Ge particles are independent of the electrolyte used [44].

The model commonly used [53] to represent this system should describe each of the anodes tested, but a quantitative analysis of the EIS spectra is not meaningful due to the complex morphology of slurry cast electrode system studied here. However, useful information may be obtained from a relative comparison between the types and magnitudes of features from anodes tested using different electrolytes or between spectra taken at various stages in the cycling of a single anode.

The EIS for the electrodes cycled in EC/DMC and FEC/DEC in the fully lithiated (10 mV) and delithiated states (1000 mV) are shown in Fig. 6a–d. Through 50 cycles, total impedance is lower in the electrode cycled in EC/DMC, most noticeably when comparing the different electrode systems in their fully lithiated state, this result correlating with the lower overpotential required to drive the stripping/plating of Li in the EC/DMC electrolyte vs. the FEC/DEC electrolyte during the testing of coin cells composed of two electrodes of Li foil (Supplementary information Fig. 6). The solution resistance for the electrode cycled in EC/DMC is nearly three times less than for the electrode cycled in FEC/DEC (6 vs 16 Ohm). The impedance through the SEI is significantly greater for the electrode cycled in FEC/DEC when in the fully-lithiated state in which the SEI is more fully formed. The impedance through the SEI depends upon the potential of the electrode because the ratio of the impedance through the SEI to the impedance due to charge transfer increases as the voltage increases. In the fully-lithiated state, the impedance through the SEI and due to charge transfer is greater in the electrode cycled in FEC/DEC. In the fully-delithiated state, the electrode cycled in EC/DMC has the larger impedance through the SEI, although in both electrodes, impedance from charge transfer is the greater factor. For the electrode cycled in FEC/DEC, an additional source of impedance was observed besides that attributed to transport through the SEI and charge transfer at the active material interface. As shown in the inset for Fig. 6d, the electrode cycled in FEC/DEC possesses an additional feature in its spectra observed at 1000 mV, a small semicircle of diameter about 5 Ohm recorded during perturbations at high frequencies. To the best of our knowledge, this has not been reported for a Ge-based or other negative electrode system.

### 3.6. SEM, TEM characterization

Electrodes were examined by SEM and TEM in their fully-delithiated state. The electrodes were removed from the coin cell in the glovebox, washed with dimethyl carbonate (DMC) and then examined by SEM. Between transfer from a vacuum tight container filled with Ar from the glovebox to the high vacuum SEM chamber, the samples were exposed to air for less than 60 seconds.

The SEM wide-field view of the electrodes cycled 100 times at 1C in EC/DMC (Fig. 7b) and FEC/DEC (Fig. 7c) shows the formation of micron-scale growths, protruding like plumes from the film surface. Using EDX mapping, the locations of these growths was correlated to the positions of large Ge particles or agglomerations within the electrode film (Supplementary information Figure SI.16). These growths on the surface of the electrode cycled in EC/DMC appear to be up to an order of magnitude larger in size than many of

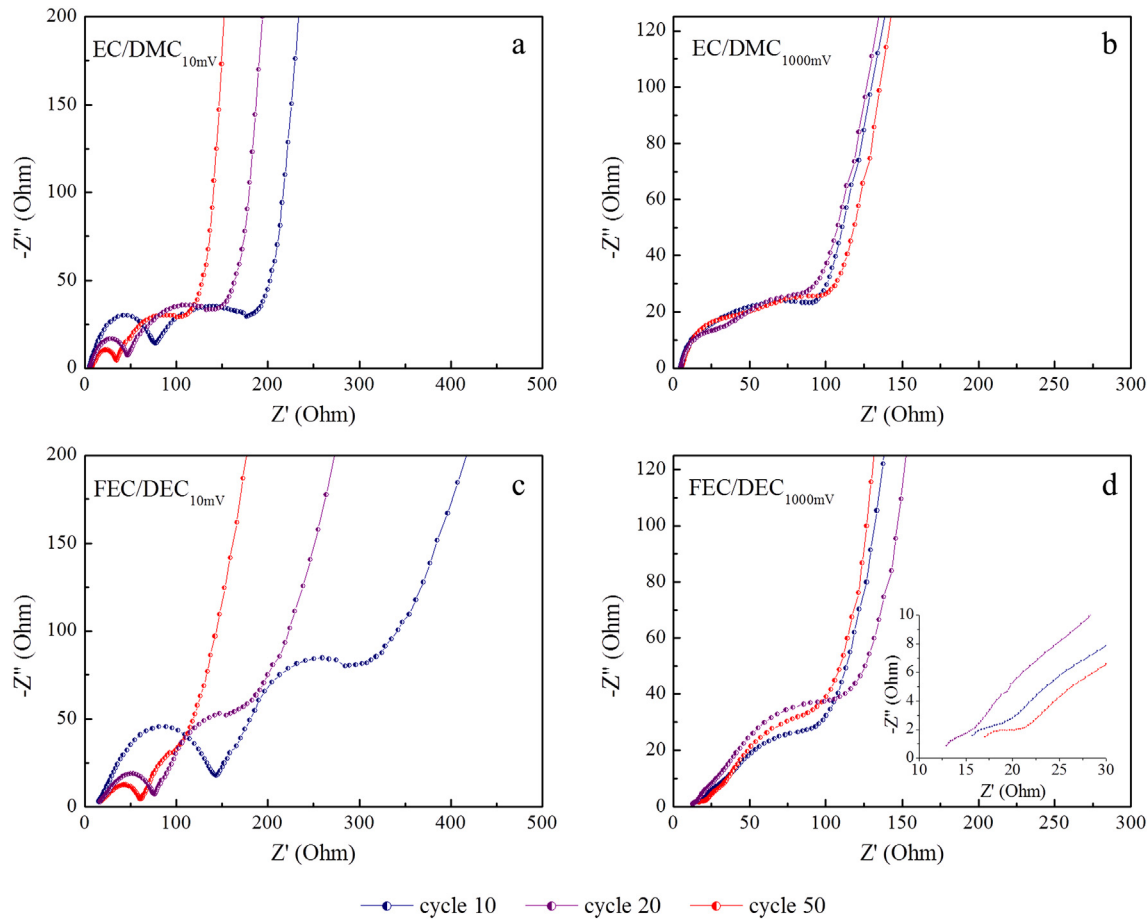


**Fig. 6.** Evolution of the electrochemical impedance spectra for Ge nanoparticle electrode cycled 10, 20 and 50 times at 1C in EC/DMC electrolyte in the (a) fully lithiated state (10 mV) and (b) fully delithiated state (1000 mV) and in the FEC/DEC electrolyte at (c) fully lithiated state (10 mV) and (d) fully delithiated state (1000 mV).

the growths appearing on the surface of the electrode cycled in FEC/DEC and have a more noticeably reticulated surface. The growths on the electrode cycled in FEC/DEC more frequently appeared mesa-like, with smoothed surfaces or, for smaller growths, the SEI surrounding the Ge nanoparticles in the electrode cycled in FEC/DEC appeared to be a collection of folded sheets forming a terraced structure (Supplementary information Figure SI.17). Using cross-sectional TEM, the growths on the electrode cycled in FEC/DEC were shown to have a similar structure compared to those cycled in EC/DMC, despite their generally more smooth exterior appearance. A high energy electron beam was used to penetrate the outer surface, revealing the porous growth on an electrode cycled in EC/DMC (Fig. 7h, Supplementary Information Figure SI.18.c). In Fig. 8, a cross section view of an organic growth on the electrode cycled in FEC/DEC is shown using TEM. Beneath the surface of the growth is a branch-like network of loosely entwined organic/inorganic components. Appearing to be fiber or sheet-like with a thickness of about 20–50 nm, this SEI growth typically begins at the surface of several Ge nanoparticles and apparently also on the surface of conductive additive Super-P Li particles. As cycling progresses, the density of the entwined components and the size of the growth increases (Supplementary information Figure SI.18.e–g). As described in Section 4.4, the expansion may occur as a consequence of evolved gas from reduction reactions near the active material surface [54,55].

From cross-sectional TEM imaging, we find that these growths are not confined to the surface of the electrode but occur

throughout the interior of the electrode film and also at the Cu foil/film interface (Fig. 9). With these, we show what we believe are the first such images that depict the SEI and its arrangement within the morphology of a slurry-cast cycled negative electrode. The roughly conformal film of SEI immediately surrounding the Ge nanoparticles (Fig. 8) was observed to be 10–50 nm. Moving further away from the particle surface, there is a noticeable transition from this smooth, more dense, semi-conformal SEI into the porous growths described above (Supplementary information Figure, SI.19). These porous growths of SEI occur throughout both electrodes considered herein, developing off of the surfaces of the electrically conductive active materials (Fig. 9a and b) and from the Cu current collector (Fig. 9c).

Due to the limited scope of a survey consisting of these TEM images which represent a cross-section of less than 100 nm of the electrode film, we believe that the several sections imaged for this study are not necessarily representative of the entire film. What was observed indicated that the interior of the electrode cycled in the EC/DMC electrolyte differed in three significant ways from the electrode cycled in FEC/DEC. One, the porous SEI growths appeared to be of greater size and more densely formed in the electrode cycled in EC/DMC (Supplementary information Figure SI.20). Two, there were larger agglomerations of Ge nanoparticles after cycling (Supplementary information Figure SI.21). Three, large regions of fractured particles were observed in the electrode cycled in EC/DMC but not in the electrode cycled in FEC/DEC (Supplementary information Figure SI.22).

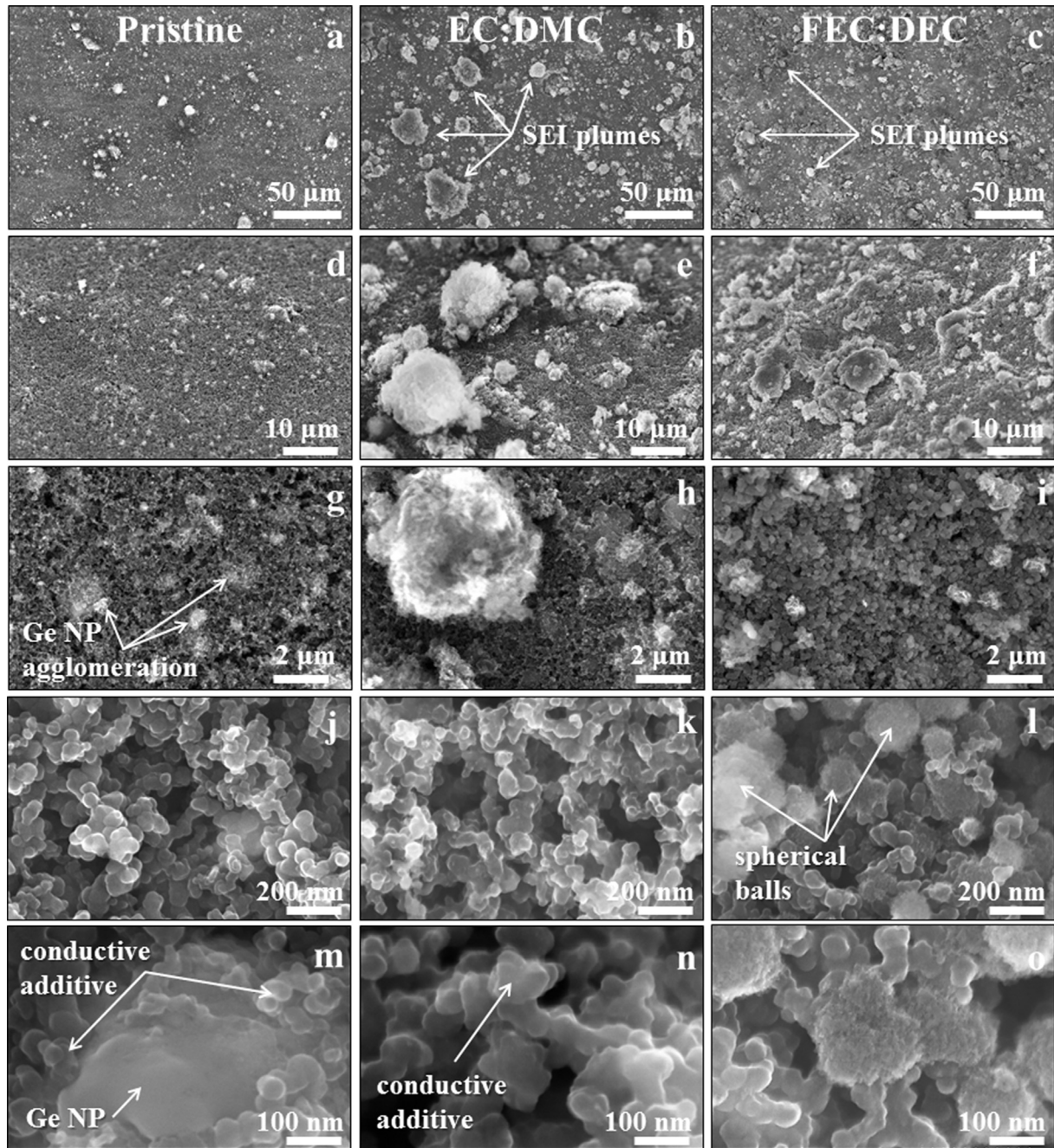


**Fig. 7.** SEM of Ge-based anode films in their pristine state, i.e., not cycled, (a, d, g, j, m) and cycled 100 times at 1C in the EC/DMC (b, e, h, k, n), and FEC/DEC (c, f, i, l, o) electrolytes. Magnifications of 500 (a, b, c), 2k (e, f, g at 37° tilt), 10k (i, j, k), 100k (j, k, l) and 200k (m, n, o) are shown.

High magnification SEM (Fig. 7k–l, n–o) shows that the morphology of the SEI film coating the conductive additive in the electrode is similar for both electrolytes tested. However, differences in cycling performance (Supplementary information Figure SI.23) and impedance measured through these SEI films (Supplementary information Figure SI.24) for the conductive additive were observed.

Surrounding the conductive additive particles in the electrode cycled in FEC/DEC, we observed unidentified spherical materials about 100–500 nm in diameter (Fig. 7 i, l, o). Using EDX, these spherical materials were determined to be composed of material other than Ge. EDX mapping was attempted but the competing signal from other species nearby and below within this highly

porous structure obscured the identity of this spherical material. These particles appeared smooth at a distance but upon high magnification inspection were observed to possess an uneven and knobby surface (Supplementary information Figure SI.25a–c).

#### 4. Discussion

##### 4.1. Cycling performance

We observed that a Ge-based electrode employing FEC/DEC as the electrolyte has a high energy density and can cycle at high C-rates with high Coulombic efficiency for a long lifetime. The stable capacity along with near 100% Coulombic efficiency achieved

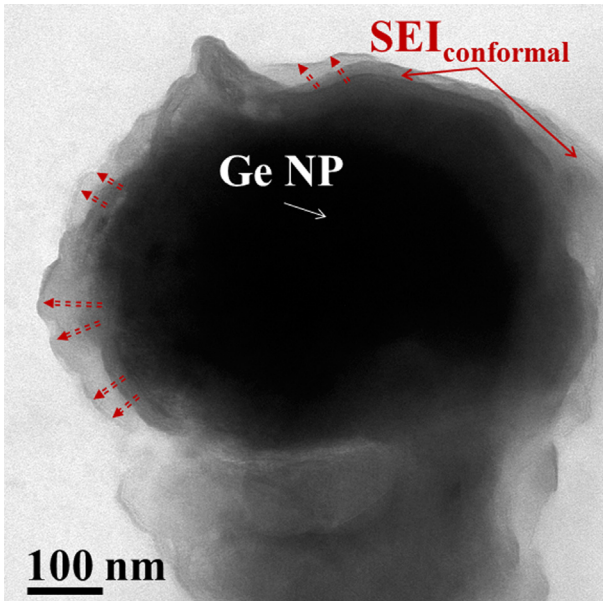


**Fig. 8.** TEM cross-section of Ge nanoparticle electrode cycled 700 times (200 cycles at 1C, 5C and 10C followed by 50 cycles at 5C and then 1C) in the FEC/DEC electrolyte. The single Ge nanoparticle is surrounded by a roughly conformal coating of SEI. The dashed arrows indicate the direction in which successive layers of SEI move to accommodate the volumetric expansion of the particle.

through 500 cycles at 10C ( $16 \text{ A g}^{-1}$ ) constant current cycling recommends the Ge nanoparticle/FEC-based electrolyte combination as an attractive electrode suited for further study for optimizing its slurry composition and scaling up its mass loading. The performance of the electrode when tested at high discharge rates (10C or 20C discharge/1C charge, [Fig. 2c](#)) and when tested for over 2500 cycles at variable rates (1C, 5C and 10C, [Fig. 2c](#)) supports this recommendation.

We believe that the performance of this anode system could be improved in terms of capacity retention at high rates by using Ge nanoparticles of a narrower size distribution and of a smaller size. The Ge particles used in this research ranged from nano to micron sized ([Supporting information Figure SI.1](#)), and consequently a fraction of the Ge particles were not fully lithiated at higher rates due to the limiting rate of Li bulk diffusion in the active material. Additionally, the applied current density per unit area of the electrode could be improved by increasing the mass fraction of the active material in the slurry and the mass loading. For example, we found electrode films made with 80 wt percent Ge nanoparticles cycled with minimal capacity fade ( $0.5 \text{ mAh g}^{-1}$  per cycle) through 100 cycles at a rate of 1C ([Supplementary information Figure SI.2](#)). Additionally, we found that an electrode made with 60 wt percent Ge nanoparticles achieved stable performance for 1000 cycles at 1C ([Supporting information Figure SI.7](#)) with a mass loading several times higher than the anodes tested and discussed in the main paper. For this particular electrode, i.e., with 60 wt percent Ge nanoparticles, the 1000th cycle capacity of  $818 \text{ mAh g}^{-1}$  (Coulombic efficiency, 99.7%) retained 93% of the 10th cycle capacity. In contrast, the nominally identical electrode cycled in EC/DMC retained less than 47% of its 10th cycle capacity after only 200 cycles.

#### 4.2. EIS and differential capacity profile

The differential capacity profile for the Ge nanoparticle electrode cycled in FEC/DEC is consistent with the cycling data, both of

which show the reversibility of this electrode system. The 1C profiles taken for the 200th, 800th and 1400th cycles ([Fig. 5](#)) are nearly identical, the difference between these being that the marginally lower capacity of the 800th and 1400th cycles is reflected in the magnitudes of the Li insertion and extraction peaks.

The differential capacity profiles for the electrode cycled in EC/DMC is likewise consistent with the cycling data, which shows the onset of capacity fade after about 20 cycles. During these first cycles for which there is no capacity fade, with the Li insertion and extraction features of the differential capacity profile are essentially unchanged in both shape and magnitude. Coinciding with the capacity fade, the two Li extraction features change, with the feature at the higher potential disappearing while the feature at the lower potential grows in magnitude, both relatively in proportion to the disappearing peak and in absolute magnitude ([Fig. 10a](#)). The only shift in this peak is to a lower potential, signifying that less overpotential is required for the Li extraction. The EIS results showing the continuous decrease in total impedance through these 50 cycles supports the interpretation of these differential capacity profiles that the kinetics of the electrode system are improving ([Fig. 6](#)). These results indicate that the thermodynamics of the electrode tested in EC/DMC change during these tens of cycles that coincide with the onset of capacity fade. When compared with the differential capacity profile of a similarly prepared electrode composed of  $\text{GeO}_2$  nanoparticles, this progressive transformation in the EC-based Ge nanoparticle electrode differential capacity profiles may be explained as indicating the gradual oxidation of the Ge nanoparticle active material ([Supplementary information Figure SI.26](#)).

After 100 cycles, the Li extraction peak initially observed above 500 mV has almost disappeared ([Fig. 10a](#)). During the subsequent 100 cycles ([Fig. 10b](#)), the changes in the differential capacity profile reflect the continuous capacity fade, with each of the Li insertion and extraction features decreasing in proportion. This behavior observed after 100 cycles fits the hypothesis which explains capacity fade in terms of either the general dislocation and dislodgement of regions of the film from the main body of the electrode and/or the electrical isolation of fractured particles when separated grains are coated with electrically insulating SEI on their freshly exposed surfaces. As the amount of electrically connected Ge nanoparticles decreases, the amplitude of the differential capacity profile diminishes in proportion to the extent of capacity fade. Although the specific current density would then also increase in terms of the amount of electrically connected Ge nanoparticles, this does not result in peak shifts due to the excellent ionic conductivity of Li ions through the EC-derived SEI (as reported in the EIS results) and fast diffusion of Li through the bulk of the Ge nanoparticles.

The lower impedance through the SEI of the Ge nanoparticle electrode cycled in EC/DMC through the first 50 cycles at 1C conflicts with recent reports of an electrolyte survey (including FEC-based electrolytes) done by Aurbach's group [40] for a Si nanowire thin film electrode and by Lin et al., [41] for a slurry cast Si-based anode. In these reports, the ionic transport is improved through better  $\text{Li}^+$  ion conducting SEI formed by FEC-based electrolytes. However, this evolution toward diminished impedance is not reflected in the cycling data for Ge-based electrodes studied here, which show stable performance for the electrode cycled in FEC/DEC and capacity fade for the electrode cycled in EC/DMC. This suggests that the impedance of transport through the surface films and related to charge transfer do not necessarily explain cycling performance data.

For both electrode systems, these EIS results coincide with the differential capacity profiles ([Fig. 4](#)) in that these show that through 50 cycles at 1C, the primary Li insertion peak for the electrode cycled in EC/DMC is found at a higher potential (lower overpotential) than

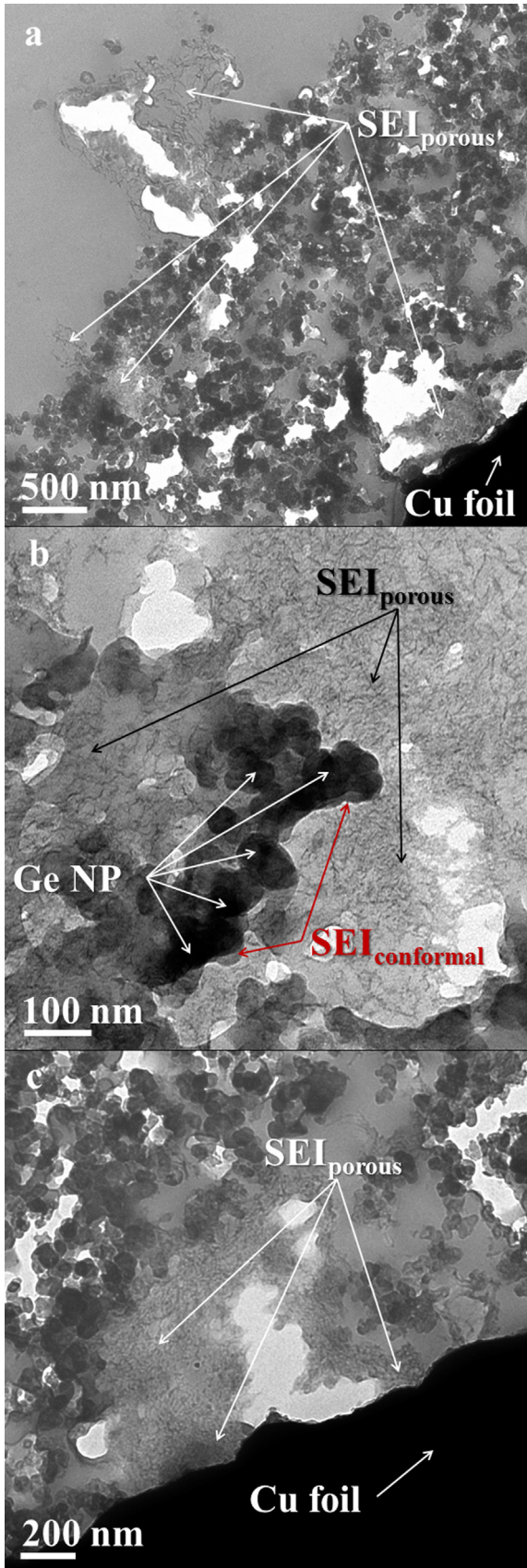


**Fig. 9.** TEM cross-section of Ge nanoparticle electrode cycled 100 times at 1C (a) in the FEC/DEC electrolyte showing the cross-sectional architecture of the electrode film comprised of Ge nanoparticles, conductive additive Super-P Li and a porous SEI

the same peak for the electrode cycled in FEC/DEC. Through 50 cycles, the decrease in impedance shown in the EIS for both electrode systems can be correlated with decreasing overpotentials required to reach this primary Li insertion peak for the electrode cycled in FEC/DEC but not for the electrode cycled in EC/DMC. For this electrode, the primary Li insertion peak remains near 165 mV for cycles 10, 20 and 50. For Li extraction from these electrode systems, there is negligible difference in the impedance spectra observed at 1000 mV, and these results correlate strongly with the minimal differences in Li extraction features for both the electrode cycled in EC/DMC and in FEC/DEC. There is no significant change in the EIS for the electrode cycled in EC/DMC which correlates to the large decrease in the size of the Li extraction feature near 515 mV for these cycles, and this suggests that the reason for the observed capacity fade is not explained by the surface transport properties of this electrode system.

#### 4.3. High rate and long cycle life performance

The cycling data for constant charge rate (1C)/variable high rate discharge testing show that Ge-based active materials tested using the FEC/DEC electrolyte are an appropriate choice for Li-ion batteries required for fast discharge applications. The nearly identical performance of electrodes tested at 10C and 20C discharge rates indicates that the charge rate, not the discharge rate, appears to be the significant limiting factor in the performance of this electrode for testing done at high current densities. We believe that this performance may be further improved not only by selecting Ge nanomaterials with an appropriate diffusion length for the rate desired but also by optimizing the electrolyte composition and separator membrane to support the rapid transport of  $\text{Li}^+$  ions. This study used Ge nanoparticles with a size distribution far wider than was advertised (listed average particle size was 70–120 nm) for this commercially available product (see [Supplementary information Figure S1.1](#)). As indicated above, the below-theoretical capacities reported in this study can be partially explained by the dimensions of the Ge active material used. The bulk diffusion rate of Li in Ge may limit electrode performance at higher C-rates, leading to particles that are not fully lithiated. Smaller Ge particles, such as those used by Lee et al., [15] or those otherwise designed with diffusion lengths appropriate for a specific range of C-rates would likely improve the capacity retention of this electrode system.

#### 4.4. SEM, TEM characterization

The combined perspectives of SEM and cross-sectional TEM used in this study depicted the structure of the electrode film and provided a means to examine the structure of the cycled anode: the Ge nanoparticles, the conductive additive (Super-P Li) and the surrounding SEI. Although the type and extent of formation of the SEI in a negative electrode is considered crucial to understanding the electrode's cycling performance, we believe the TEM images shown herein are the first to reveal the nature and scope of growth of SEI within a cycled slurry cast electrode. Embedding the cycled electrode within epoxy, which is subsequently polymerized and hardened, preserves the chemical integrity of the electrode film and SEI from contaminating species formed when the sample is exposed to air. The structural integrity of the electrode film is also well preserved due to the hardened epoxy supporting the porous

indicated by arrows, (b) in the EC/DMC electrolyte showing Ge nanoparticles in the electrode film surrounded by a roughly conformal coating of SEI that transitions into porous SEI and (c) in the FEC/DEC electrolyte showing porous SEI growth from the Cu foil current collector.

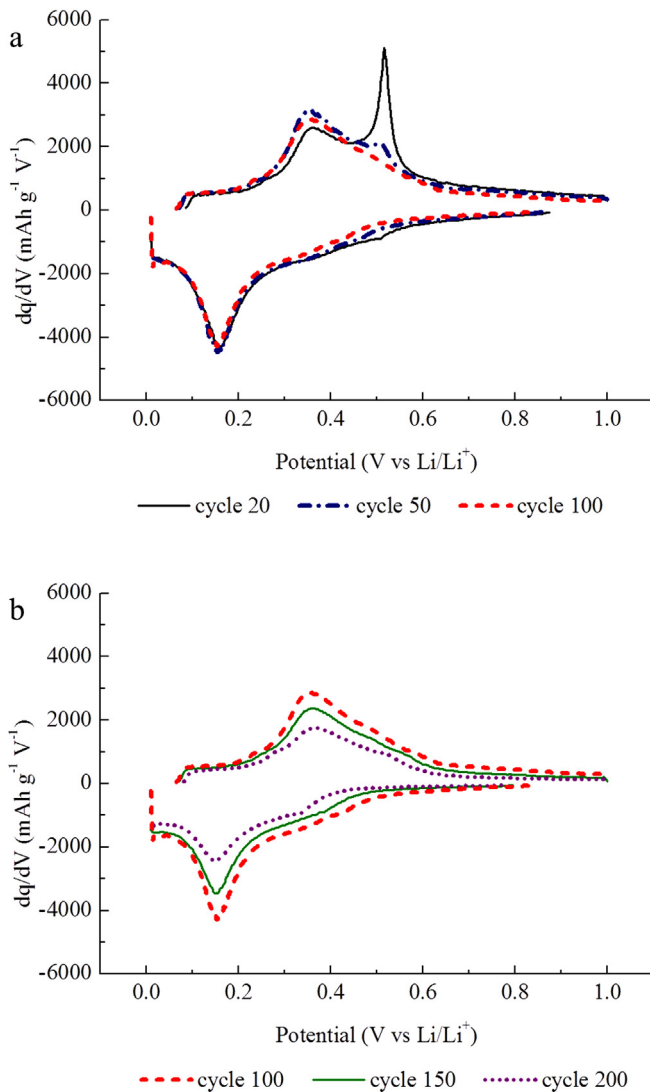


**Fig. 10.** Differential capacity profiles for the Ge nanoparticle electrode cycled in EC/DMC at 1C (a) cycles 20, 50 and 100 and (b) cycles 100, 150 and 200.

electrode architecture and because of the non-destructive nature of ultra-microtome sectioning. Using cross-sectional TEM, we observed what we believe are two types of SEI growth. One is a layered and more densely formed material, conformally surrounding the Ge nanoparticle (or conductive additive). The other observed variety of SEI developed off of both the electrically conductive particles and from the surface of the Cu foil current collector. Porous in nature, with fiber-like strands, we believe the structure of this SEI may be partially attributed to the motion of volumetric expansion and contraction of the Ge nanoparticles. Because of their microns-dimension and directional growth along an axis paralleling the gravitational rise of evolved gas bubbles ( $\text{CO}_2$ ,  $\text{H}_2$ ) [54,55] it may be that the evolved gas expands the SEI to the morphology observed.

Failure mode mechanisms, such as the extent of particle agglomeration and particle fracture are also indicated by TEM images. Here we observe evidence for both the agglomeration of active material nanoparticles (Supplementary information Figure SI.21) and Ge particle fracturing (Supplementary information Figure SI.22). Due to the variety of sizes and shapes of the commercially used Ge nanopowder, the ability to contrast

the changed morphology of the particle after several cycles with its uncycled condition is limited. With careful materials selection, and using image processing techniques to quantitatively assess the extent of particle agglomeration and fracture, a more comprehensive study of the cycled, slurry-cast electrode film may be done. Herein we demonstrate the first reported instance of cross-sectional TEM as a tool for characterizing the changes in the structure of the nanoparticle network and growth of SEI after cycling.

## 5. Conclusions

Ge nanoparticle based slurry cast electrodes were tested with PAA binder in 1 M  $\text{LiPF}_6$  EC/DMC or FEC/DEC electrolytes. The critical factor determining the cycling performance of the anode was determined to be the use of fluoroethylene carbonate (FEC) as a co-solvent in the electrolyte solution. For this FEC-based electrode system, we report long-term, high capacity/Coulombic efficiency and stable cycling results for a selection of high C-rate tests. Throughout a 2500 cycle (alternating 200-cycle, variable high rate) test done at 1C, 5C and 10C, we found stable capacities/high Coulombic efficiencies near  $1152 \text{ mAh g}^{-1}$ /99.7%,  $706 \text{ mAh g}^{-1}$ /99.2% and  $423 \text{ mAh g}^{-1}$ /99.7%. Continuous testing at 10C showed a capacity near  $700 \text{ mAh g}^{-1}$  with an average Coulombic efficiency of 100% through 500 cycles. Capacities over  $1000 \text{ mAh g}^{-1}$  were observed when discharging the electrode at up to 20C while charging at 1C and a capacity of  $425 \text{ mAh g}^{-1}$  was achieved for a discharge rate of 50C. These results and our preliminary work for a similar electrode system with higher mass content and mass loadings (Supplementary information Figures SI.2 and SI.7) successfully demonstrate that for the Ge-based slurry cast electrode, the attractive properties of this Li-ion anode material – Li diffusion rate, electrical conductivity and theoretical capacity – can be used to create an electrode system which is a candidate for optimization and scale-up based upon its performance in several of the significant battery parameters of interest: maximum specific power output, gravimetric and volumetric energy densities, Coulombic efficiency and cycle life. These cycling improvements obtained by the use of the FEC-based electrolyte in a Ge-based electrode complements the recent progress in slurry cast Ge-based electrode research which has focused on improving performance through structural and chemical modifications to the structure of the active material. Differential capacity profiles provided evidence of the improved thermodynamic stability of the electrode system, which we suggest may be a result of the enhanced preservation of Ge active material by a FEC-derived SEI that stabilizes the electrode against oxidation. Through the use of cross-sectional TEM imaging, we characterize the evolution of the structure of the improved electrode cycled with the FEC-based electrolyte by considering the type and extent of SEI growth, particle agglomeration and fracturing within the cycled electrode film.

## Acknowledgments

The authors declare no competing interest. Financial support of this research was provided by the Robert A. Welch Foundation (CBM F-1436, AH F-1131, BAK F-1464). K.C.K. acknowledges the NSF Graduate Research Fellowship Program for financial support. K.C.K. especially thanks Dr. Elmer Klavetter, as well as Paul R. Abel and Mark Cassarra for their contributions to this study.

## Appendix A. Supplementary data

Supplementary data related to this article can be found at <http://dx.doi.org/10.1016/j.jpowsour.2013.02.091>.

## References

- [1] J.B. Goodenough, Y. Kim, *Chemistry of Materials* 22 (2009) 587–603.
- [2] L. Baggetto, E.J.M. Hensen, P.H.L. Notten, *Electrochimica Acta* 55 (2010) 7074–7079.
- [3] X.H. Liu, S. Huang, S.T. Picraux, J. Li, T. Zhu, J.Y. Huang, *Nano Letters* 11 (2011) 3991–3997.
- [4] D. Wang, Y.-L. Chang, Q. Wang, J. Cao, D.B. Farmer, R.G. Gordon, H. Dai, *Journal of the American Chemical Society* 126 (2004) 11602–11611.
- [5] J. Graetz, C.C. Ahn, R. Yazami, B. Fultz, *Journal of The Electrochemical Society* 151 (2004) A698–A702.
- [6] C.S. Fuller, J.C. Severiens, *Physical Review* 96 (1954) 21–24.
- [7] M.-H. Park, Y. Cho, K. Kim, J. Kim, M. Liu, J. Cho, *Angewandte Chemie International Edition* 50 (2011) 9647–9650.
- [8] R. Huggins, W. Nix, *Ionics* 6 (2000) 57–63.
- [9] L. Baggetto, P.H.L. Notten, *Journal of The Electrochemical Society* 156 (2009) A169–A175.
- [10] U. Kasavajjula, C. Wang, A.J. Appleby, *Journal of Power Sources* 163 (2007) 1003–1039.
- [11] L.Y. Beaulieu, S.D. Beattie, T.D. Hatchard, J.R. Dahn, *Journal of The Electrochemical Society* 150 (2003) A419–A424.
- [12] W.-J. Zhang, *Journal of Power Sources* 196 (2011) 13–24.
- [13] H. Wu, Y. Cui, *Nano Today* 7 (2012) 414–429.
- [14] J. Wang, N. Du, H. Zhang, J. Yu, D. Yang, *Journal of Materials Chemistry* 22 (2012) 1511–1515.
- [15] H. Lee, M.G. Kim, C.H. Choi, Y.-K. Sun, C.S. Yoon, J. Cho, *The Journal of Physical Chemistry B* 109 (2005) 20719–20723.
- [16] M.-H. Park, K. Kim, J. Kim, J. Cho, *Advanced Materials* 22 (2010) 415–418.
- [17] M.-H. Seo, M. Park, K.T. Lee, K. Kim, J. Kim, J. Cho, *Energy & Environmental Science* 4 (2011) 425–428.
- [18] A.M. Chockla, K. Klavetter, C.B. Mullins, B.A. Korgel, *ACS Applied Materials & Interfaces* 4 (2012) 4658–4664.
- [19] S. Yoon, C.-M. Park, H.-J. Sohn, *Electrochemical and Solid-State Letters* 11 (2008) A42–A45.
- [20] D.-J. Xue, S. Xin, Y. Yan, K.-C. Jiang, Y.-X. Yin, Y.-G. Guo, L.-J. Wan, *Journal of the American Chemical Society* 134 (2012) 2512–2515.
- [21] H. Lee, H. Kim, S.-G. Doo, J. Cho, *Journal of The Electrochemical Society* 154 (2007) A343–A346.
- [22] G. Jo, I. Choi, H. Ahn, M.J. Park, *Chemical Communications* 48 (2012) 3987–3989.
- [23] L.C. Yang, Q.S. Gao, L. Li, Y. Tang, Y.P. Wu, *Electrochemistry Communications* 12 (2010) 418–421.
- [24] B. Wu, A. Heidelberg, J.J. Boland, *Nature Materials* 4 (2005) 525–529.
- [25] L. Lu, M.L. Sui, K. Lu, *Science* 287 (2000) 1463–1466.
- [26] C.K. Chan, X.F. Zhang, Y. Cui, *Nano Letters* 8 (2007) 307–309.
- [27] C.K. Chan, H. Peng, G. Liu, K. McIlwrath, X.F. Zhang, R.A. Huggins, Y. Cui, *Nature Nanotechnology* 3 (2008) 31–35.
- [28] A.S. Arico, P. Bruce, B. Scrosati, J.-M. Tarascon, W. van Schalkwijk, *Nature Materials* 4 (2005) 366–377.
- [29] K.T. Lee, J. Cho, *Nano Today* 6 (2011) 28–41.
- [30] R. Ruffo, S.S. Hong, C.K. Chan, R.A. Huggins, Y. Cui, *The Journal of Physical Chemistry C* 113 (2009) 11390–11398.
- [31] H. Wu, G. Chan, J.W. Choi, I. Ryu, Y. Yao, M.T. McDowell, S.W. Lee, A. Jackson, Y. Yang, L. Hu, Y. Cui, *Nature Nanotechnology* 7 (2012) 310–315.
- [32] B. Hertzberg, A. Alexeev, G. Yushin, *Journal of the American Chemical Society* 132 (2010) 8548–8549.
- [33] M.T. McDowell, S.W. Lee, I. Ryu, H. Wu, W.D. Nix, J.W. Choi, Y. Cui, *Nano Letters* 11 (2011) 4018–4025.
- [34] H. Wu, G. Zheng, N. Liu, T.J. Carney, Y. Yang, Y. Cui, *Nano Letters* 12 (2012) 904–909.
- [35] L. Hu, H. Wu, Y. Gao, A. Cao, H. Li, J. McDough, X. Xie, M. Zhou, Y. Cui, *Advanced Energy Materials* 1 (2011) 523–527.
- [36] D. Wang, Z. Yang, F. Li, D. Liu, X. Wang, H. Yan, D. He, *Materials Letters* 65 (2011) 1542–1544.
- [37] N.G. Rudawski, B.L. Darby, B.R. Yates, K.S. Jones, R.G. Elliman, A.A. Volinsky, *Applied Physics Letters* 100 (2012) 083111–083114.
- [38] K.H. Seng, M.-H. Park, Z.P. Guo, H.K. Liu, J. Cho, *Angewandte Chemie International Edition* 51 (2012) 5657–5661.
- [39] A.M. Chockla, K.C. Klavetter, C.B. Mullins, B.A. Korgel, *ACS Applied Materials & Interfaces* 4 (2012) 4658–4664.
- [40] V. Etacheri, O. Haik, Y. Goffer, G.A. Roberts, I.C. Stefan, R. Fasching, D. Aurbach, *Langmuir* 28 (2011) 965–976.
- [41] Y.-M. Lin, K.C. Klavetter, P.R. Abel, N.C. Davy, J.L. Snider, A. Heller, C.B. Mullins, *Chemical Communications* 48 (2012) 7268–7270.
- [42] H. Nakai, T. Kubota, A. Kita, A. Kawashima, *Journal of The Electrochemical Society* 158 (2011) A798–A801.
- [43] N.-S. Choi, K.H. Yew, K.Y. Lee, M. Sung, H. Kim, S.-S. Kim, *Journal of Power Sources* 161 (2006) 1254–1259.
- [44] V. Etacheri, U. Geiger, Y. Goffer, G.A. Roberts, I.C. Stefan, R. Fasching, D. Aurbach, *Langmuir* 28 (2012) 6175–6184.
- [45] A. Magasinski, B. Zdryko, I. Kovalenko, B. Hertzberg, R. Burtovyy, C.F. Huebner, T.F. Fuller, I. Luzinov, G. Yushin, *ACS Applied Materials & Interfaces* 2 (2010) 3004–3010.
- [46] J.W. Choi, L. Hu, L. Cui, J.R. McDonough, Y. Cui, *Journal of Power Sources* 195 (2010) 8311–8316.
- [47] A.M. Chockla, K.C. Klavetter, C.B. Mullins, B.A. Korgel, *Chemistry of Materials* 24 (2012) 3738–3745.
- [48] J. Goodenough, *Journal of Solid State Electrochemistry* 16 (2012) 2019–2029.
- [49] D. Djian, F. Alloin, S. Martinet, H. Lignier, J.Y. Sanchez, *Journal of Power Sources* 172 (2007) 416–421.
- [50] G.A. Umeda, E. Menke, M. Richard, K.L. Stamm, F. Wudl, B. Dunn, *Journal of Materials Chemistry* 21 (2011) 1593–1599.
- [51] J.B. Goodenough, Y. Kim, *Journal of Power Sources* 196 (2011) 6688–6694.
- [52] A.S. Jing Li, R.J. Sanderson, T.D. Hatchard, R.A. Dunlap, J.R. Dahn, *Journal of The Electrochemical Society* 156 (2009) A283–A288.
- [53] J. Liu, A. Manthiram, *Chemistry of Materials* 21 (2009) 1695–1707.
- [54] J.H. Seo, J. Park, G. Plett, A.M. Sastry, *Electrochemical and Solid-State Letters* 13 (2010) A135–A137.
- [55] S.S. Zhang, *Journal of Power Sources* 162 (2006) 1379–1394.